RSC Advances

PAPER

Cite this: *RSC Adv.*, 2021, **11**, 37801

Structural, optical and photocatalytic properties of mesoporous CuO nanoparticles with tunable size and different morphologies†

Mohamed I. Said, *[a] A. A. Othman[b] and Esraa M. Abd elhakeem[b]

Nanomaterials with controllable particle size and shape have fascinating properties. Herein, CuO nanoparticles (NPs) with controlled particle size and morphology are obtained *via* a simple co-precipitation approach. Variation of the reaction medium composition steers the variation of both particle size and morphology of the CuO NPs. The reaction was performed in ethanol–water solutions with different volume to volume ratios (v/v%) *i.e.* 0, 25, 50, and 100%. XRD of the obtained samples revealed a drop in their particle size from ~13 to ~7 nm when the aqueous medium is entirely replaced by the ethanolic medium. TEM and HR-TEM investigations have pointed to the formation of CuO NPs with rod-like shapes in water (diameter = 15 nm and length = 200 nm). Whereas, spherical NPs with a diameter of 7.2 nm are obtained in ethanol. Structural analysis of CuO samples obtained in different media was done applying the Rietveld method. The volume of the monoclinic unit cell of CuO is increased to 81.869 Å^3 when water (81.207 Å^3) is completely substituted by ethanol. Moreover, the internal local strain (ε) and the dislocation density (δ) values increase from 2.78 × 10^{-3} to 4.64 × 10^{-3} and 0.592 × 10^6 to 1.93 × 10^6 line per m^2, respectively by changing from aqueous to ethanolic medium. The optical band gap (E_g) determined using Tauc's equation for the direct transition is increased from 2.2 to 2.65 eV when water is totally replaced by ethanol. The feasibility of both CuO samples as photocatalysts for the degradation of Congo red was tested. CuO prepared in pure water showed remarkably high efficiency during the first 25 min of illumination. Both samples showed complete dye removal after 35 min. Ultimately, this work presents a simple and green approach for the preparation of CuO NPs with tunable particle size, varied morphological shapes, high surface area, and different structural and optical properties merely through controlling the ethanol content in water.

Received 20th June 2021
Accepted 27th October 2021

DOI: 10.1039/d1ra04780a

rsc.li/rsc-advances

1. Introduction

In the last few decades, considerable attention has been paid to the synthesis of nano-size materials. Among these materials, transition metal oxides (TMOs) are of great interest owing to their various applications. Copper oxides represent a significant class of transition metal oxides. Cupric oxide (CuO) with the mineral name tenorite is a black solid and is one of the two stable oxides of copper, the other one is Cu_2O (cuprous oxide). CuO has a monoclinic unit cell with space group $C2/c$ in which each Cu atom is coordinated by four oxygen atoms.

CuO is an important, low-cost, and nontoxic p-type semiconductor material with a band gap of 1.2 eV.[1] Understanding of the physical and chemical properties of CuO generates much interest due to its wide range of applications in gas sensors,[2] biosensors,[3] photo-detectors,[4] magnetic storage media,[5] supercapacitors,[6] photocatalysis,[7] removal of inorganic pollutants[8,9] and antimicrobial applications.[10]

Various preparation techniques have been developed for the synthesis of CuO nanostructures such as sol–gel,[11] hydrothermal,[12] microwave-assisted,[13] thermal decomposition of coordination polymers,[14] and colloidal chemical precipitation.[15] The sol–gel method is one of the utmost widespread chemical solution approaches, it shows the advantages of scalability, energy efficiency, and cost-effectiveness for the synthesis of nanostructured metal oxides with controlled morphology and growth conditions.[16,17] Especially, it has been used for the formation of highly stoichiometric homogenous, and fine metal oxide nanostructures such as nanorods,[18,19] nanoflakes,[20] nanotubes,[18,21] and nanofibers.[22] To the best of our knowledge, no reports exist for the sol–gel based green synthesis method, that integrate sols and a solvent-induces shape-controlled formation in ethanol–water solution at low temperature to form smaller size and large surface CuO nanomaterials.

Previous studies have shown that metal oxide nanoparticles with tunable particle size *e.g.* Mn_3O_4 and Fe_3O_4 can be

[a]*Chemistry Department, Faculty of Science, Assiut University, 71516, Assiut, Egypt. E-mail: moh_chem1@yahoo.com; mohamedali123@aun.edu.eg; Tel: +20-1009288594*

[b]*Physics Department, Faculty of Science, Assiut University, 71516, Assiut, Egypt*

† Electronic supplementary information (ESI) available. See DOI: 10.1039/d1ra04780a

synthesized by sol–gel methods in ethanol–water solutions.[23,24] A facile sol–gel method has been established by Rathnayake *et al.*[25] to synthesize shape-controlled ZnO nanostructures. In this approach, both of the solvent polarity propelled self-assembly and solvothermal crystal growth process have played a crucial role for formation of shape-controlled ZnO nanomaterials. They showed that the polarity difference and surface adhesion of an organic solvent govern the growth of nanocrystals. In this sense, solvent molecules are acting as surfactants that adsorb onto surfaces of the growing crystallites.

In this work, we extend and modify a consistent sol–gel method that associates the production of CuO nanocrystals sol and shape-controlled process (solvent-induced process) to make neat CuO nanostructures in ethanol–water solutions with different contents at 100 °C. We can form CuO nanostructures with various morphologies and particle sizes in addition to the engineered band gap and large surface area using this one-pot synthesis method without affecting their crystalline structure or compositions.

Congo red (CR) is a benzidine-based anionic disazo dye generally utilized in the manufacturing of silk clothing. It has toxic properties to various organisms and is assumed to be carcinogenic and mutagenic. CR contaminated effluents are also produced from textiles, printing and dyeing, paper, rubber, plastic industries, and so on.[26] It has a stable structure and thus it biodegrades hardly.[27] Consequently, there is a raised demand for developing efficient remediation technologies to get rid of such poisonous dye. In this work we used the CuO NPs prepared in pure water and pure ethanol as heterogeneous photocatalysts for the remediation of Congo red contaminated-water. Highly efficient removal for the dye color was achieved in 5 min.

Eventually, we can emphasize that the method introduced in this work is a "green synthesis" in which we use an ecologically favorable and benign substances, with energy effective chemical method. As compared to other methods, our method offers a scale-up, processable, reproducible, and reliable synthesis of highly efficient CuO photocatalysts, which utilizes either sophisticated procedures or highly toxic solvents and additives. Furthermore, the produced CuO nanomaterials in this work adopt very high surface area compared to the other reported ones.

2. Experimental

2.1. Materials

All reagents were of analytical grade. Copper(II)acetate monohydrate was purchased from Sigma-Aldrich. Sodium hydroxide, ethyl alcohol (≥99.5) and Congo red were purchased from Merck and were used as received.

2.2. Synthesis of CuO NPs

In a typical procedure, 5 mmol of $Cu(OAc)_2 \cdot H_2O$ and 20 mmol NaOH were introduced in a 500 mL round flask, then 100 mL of distilled water was added. Thereafter, the whole mixture was maintained under reflux in an oil bath at 100 °C for 1 h. After cooling to room temperature, the black precipitate was separated by centrifugation (6000 rpm) and washed with water several times. The sample was dried at 60 °C for 3 h.

The same experimental procedures as above were repeated by replacing water partially with ethanol. Different volume ratios of EtOH/H_2O (v/v) were used; 0%, 25, 50% and 100%.

The yield of CuO NPs obtained in 0%, 50% and 100% EtOH was 95, 97 and 100%, respectively.

2.3. Physical techniques

X-ray diffraction (XRD) structural investigations for the obtained CuO NPs were carried out employing a Philips-type diffractometer (1700 version with H. T. P. W 1730/104 KVA and the anode was Cu Kα; $\lambda = 1.54180$ Å). The parameters for the acquisition of the XRD diffractograms are: a step size of 0.061°, time per step of 0.60 s, total time per step is 93.0 s and sample rotation 15.0° min^{-1}.

FT-IR of the prepared CuO NPs was recorded on a Shimadzu IR-470 spectrophotometer from 4000–400 cm^{-1} by means of KBr disc technique. The UV-vis spectra of the nanoparticles suspended in water were recorded utilizing a Shimadzu UV-2101 PC spectrophotometer. The suspensions were sonicated for 10 min prior to the measurements.

Thermal behavior of the CuO samples prepared in pure water and pure ethanol was studied utilizing a Shimadzu Thermal Analyzer (TA60H, Japan) in an air flow (40 mL min^{-1}). TGA/DTA analysis was done from room temperature to 700 °C with heating rate of 5 °C min^{-1}.

Transmission electron microscope (TECNAI G^2spirit TWIN microscope, operating at 120 kV and conducted by VELETA camera) was employed to determine the crystallinity, size and morphological shape of the prepared copper oxide NPs.

Nitrogen adsorption–desorption isotherms were measured at −196 °C by Quantachrome Instrument Corporation, USA (Model Nova 3200). Test samples were thoroughly out gassed for 2 h at 150 °C.

Photocatalysis was performed using UV-LED lamp from Nichia; model NVMUR008A with a power of 11.8 W and wavelength of 365 nm.

2.4. Photocatalytic degradation

In a typical procedure, 75 mL of an aqueous Congo red solution with an initial concentration of 5 ppm was mixed with 10 mg of CuO NPs (prepared in pure ethanol and pure water) as heterogeneous photocatalyst. Before irradiation, the mixture was stirred for 30 min in dark to reach an adsorption–desorption equilibrium. The mixture was then irradiated *via* a UV-LED lamp (11.8 W and $\lambda = 365$ nm). At regular time interludes parts of a 5 mL of the reaction mixture were taken, whilst the suspended photocatalyst was removed by centrifugation (6000 rpm). Ultimately, the residual Congo red concentration in the filtrate was determined using UV-vis spectrophotometer at 499 nm.

3. Results and discussion

3.1. XRD analysis

According to the sol–gel method, the formation of CuO NPs occurs through two consecutive steps. Firstly, the formation of copper hydroxide from the reaction of copper(II) acetate and

sodium hydroxide. Secondly, the heat-assisted transformation of metastable copper hydroxide to CuO as depicted by the following equations:

$$Cu(CH_3COO)_2 + 2NaOH \rightarrow Cu(OH)_2 + 2CH_3COONa \quad (1)$$

$$Cu(OH)_2 \rightarrow CuO + H_2O \quad (2)$$

The products of the former reactions obtained using different ratios of EtOH/H_2O were characterized by XRD analysis (Fig. 1). All patterns are clearly indexed to the pristine phase of CuO with a monoclinic unit cell and space group $C2/c$. Typically, the reflections found at $2\theta = 32.72°$, 35.76°, 38.87°, 49.11°, 53.74°, 58.38°, 61.72°, 66.51° and 68.25° are related to (110), (−111), (111), (−202), (020), (202), (−113), (−311) and (220) plane orientations of CuO (JCPDS 80-1268).[28]

The general feature that one can observe from the powder patterns is the broadening and decreasing of the intensity of the reflections with increasing of % EtOH in water. This observation reflects the drop in the particle size of the CuO NPs. The average crystallite size of the obtained CuO samples was estimated by applying Scherrer's formula. The relationship between the ethanol content in water and the average crystallite size was plotted and Fig. 2 was received. It is obvious that the size of CuO NPs drops almost linearly with increasing of ethanol content in water. CuO NPs with an average size (D) of 13 nm were produced in pure H_2O whilst CuO NPs with an average size (D) of 7 nm were obtained in pure EtOH.

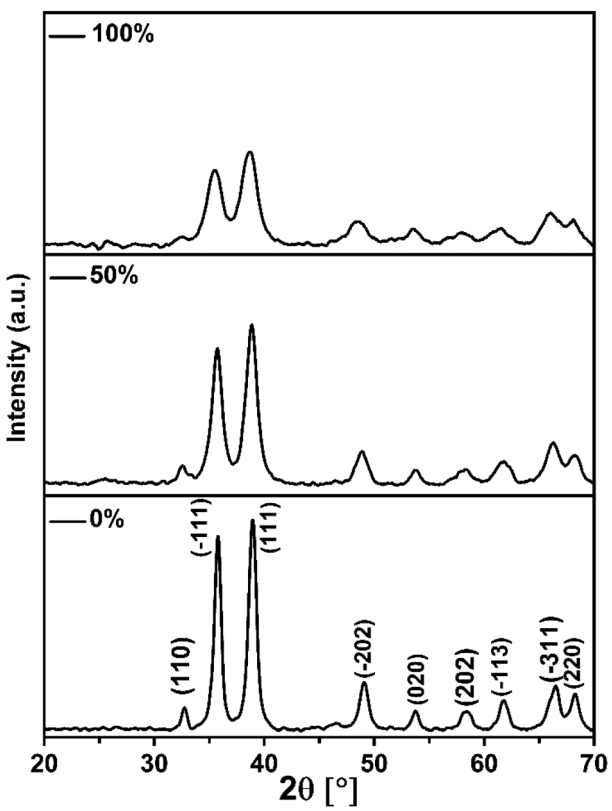

Fig. 1 XRD patterns of CuO samples prepared using co-precipitation reaction in EtOH/H_2O solutions with different v/v ratio: 0%, 50% and 100%.

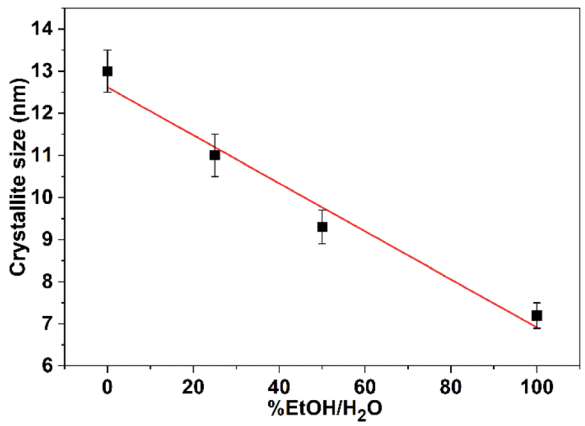

Fig. 2 Effect of variation of ethanol content in water on the average crystallite size of CuO NPs.

The drop of the particle size of CuO as a result of increasing the ethanol content in water could be explained based on the difference in the surface energies of the crystal facets of CuO NPs. Ethanol and water will adhere to each crystal facets differently owing to the difference in their polarities. Hence, ethanol acts as a surfactant that minimizes the surface energies of the crystal facets, yielding different size and shape CuO nanostructures. This explanation will be further established by IR results in the next section.

Furthermore, decreasing of the dielectric constant (ε) of the reaction solvent may result in a decrease in the particle size of the obtained product.[24] The reduction in the size of nanocrystals while using a low dielectric constant solvent such as ethanol ($\varepsilon = 25.10$ at 293 K) can be ascribed to the decrease in the solubility product which in turn facilitates the homogeneous nucleation. Consequently, a product with a higher number of particles is obtained due to the small dielectric constant of ethanol compared to that of water ($\varepsilon = 80.2$ at 293 K).

3.2. IR analysis

IR spectrum of CuO NPs (Fig. 3) obtained in pure water shows three absorption bands at 418, 490, and 605 cm^{-1}, which can be

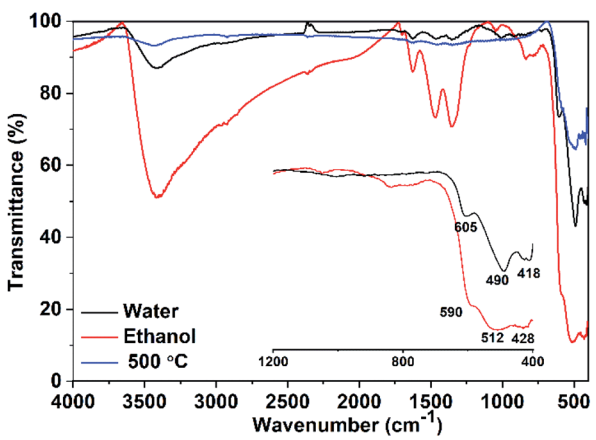

Fig. 3 IR spectra of CuO samples prepared using pure water and pure ethanol.

attributed to the Au, Bu, and another Bu modes of the monoclinic-phase CuO, respectively.[29] The absorption band located at ~605 cm^{-1} can be related to a Cu–O stretching along the [$\bar{1}$01] direction, whereas the band observed at ~490 cm^{-1} might be attributed to a Cu–O stretching along [101] direction.[30] On the other hand, a shift in the peak positions is observable (Fig. 3) for the sample obtained in pure ethanol, which could be a result of the particle size and/or morphology change. Moreover, the samples show additional peaks in the range of 1350–1670 cm^{-1}. These peaks are more pronounced for the sample obtained in pure ethanol than those for the sample obtained in pure water. They can be attributed to the symmetric and asymmetric carbonyl stretching vibrations of unreacted acetate ions from copper salt (physically adsorbed on the nanoparticle surface). For the sample obtained in pure ethanol, the shift in the peak positions may indicate the adhesion of ethanol to the surface of the crystal facets. Also, the presence of a strong absorption band at 3500 cm^{-1} that is not present in the sample prepared in water, suggests the presence of strong OH groups of ethanol. The bands located in the range of 1350–1670 cm^{-1} as well as the strong band at 3500 cm^{-1} are completely disappeared when the sample obtained in ethanol is heated to 500 °C. It is apparent from IR spectra that ethanol and acetate ions bound to the surface of the NPs are removed after heating. The former results represent an additional evidence for the existence of ethanol that may act as a surfactant and minimize the surface energies of selective facets.

For both samples, there are no observable active modes from Cu_2O in the IR spectra which prove that the samples are pure CuO with a monoclinic structure.

3.3. Morphological investigation

The impact of ethanol content on the morphology of the as-prepared CuO NPs was examined using TEM, TEM images are depicted in Fig. 4a and 5a. It is quite obvious that ethanol has a large influence on the shape of the obtained nanoparticles. Using pure water CuO NPs with rod-like shapes are produced, the rods are approximately 200 nm in length and 15 nm in diameter. The formation of such rods is an evident for anisotropic growth of CuO NPs. In pure ethanol CuO NPs adopt sphere-like structures with an average diameter of 7 nm, the particles are growing isotropically in this case. SAED pattern of the sample obtained in pure water is shown in Fig. 4b, the ring pattern is indexed which confirms the phase purity of the CuO nanorods as shown by XRD results. Furthermore, it indicates the polycrystalline nature of the obtained nanoparticles. The same conclusions can be extracted from the SAED pattern (Fig. 5b) of CuO nanoparticles formed in pure ethanol.

HR-TEM images of the CuO nanorods and nanospheres illustrated in Fig. 4c and 5c reflect the crystalline nature also. They have uniform structures with a periodic fringe spacing of 0.32 nm (Fig. 4d and 5d), which corresponds to the interplanar

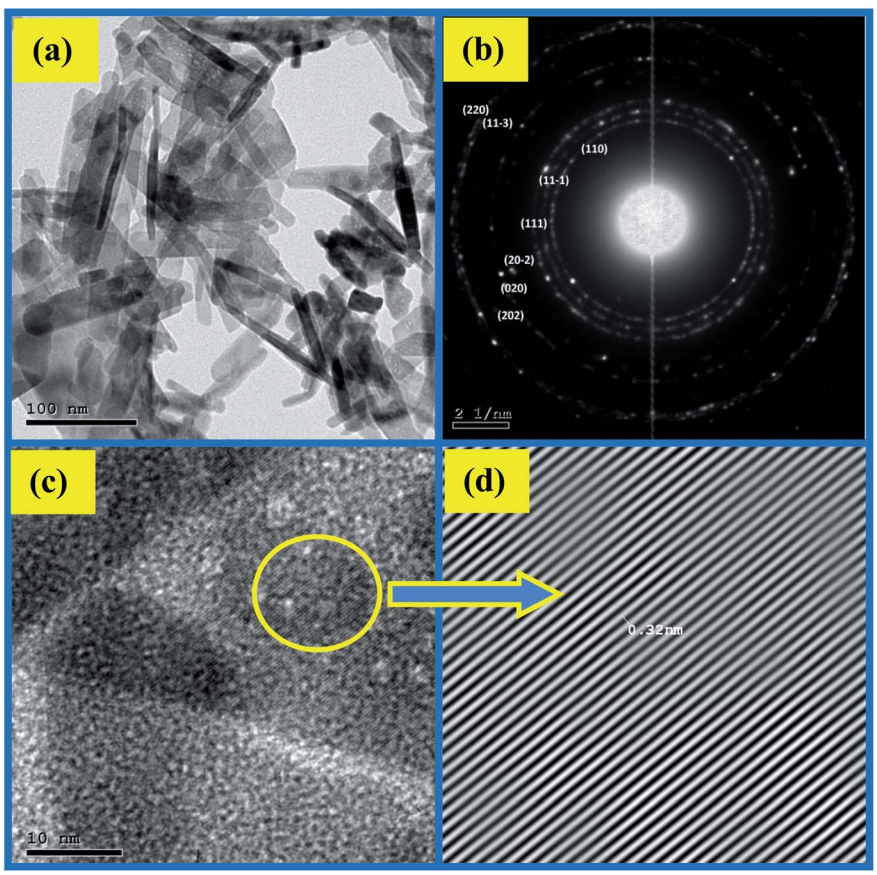

Fig. 4 (a) TEM, (b) SAED and (c and d) HR-TEM of CuO sample prepared in pure water.

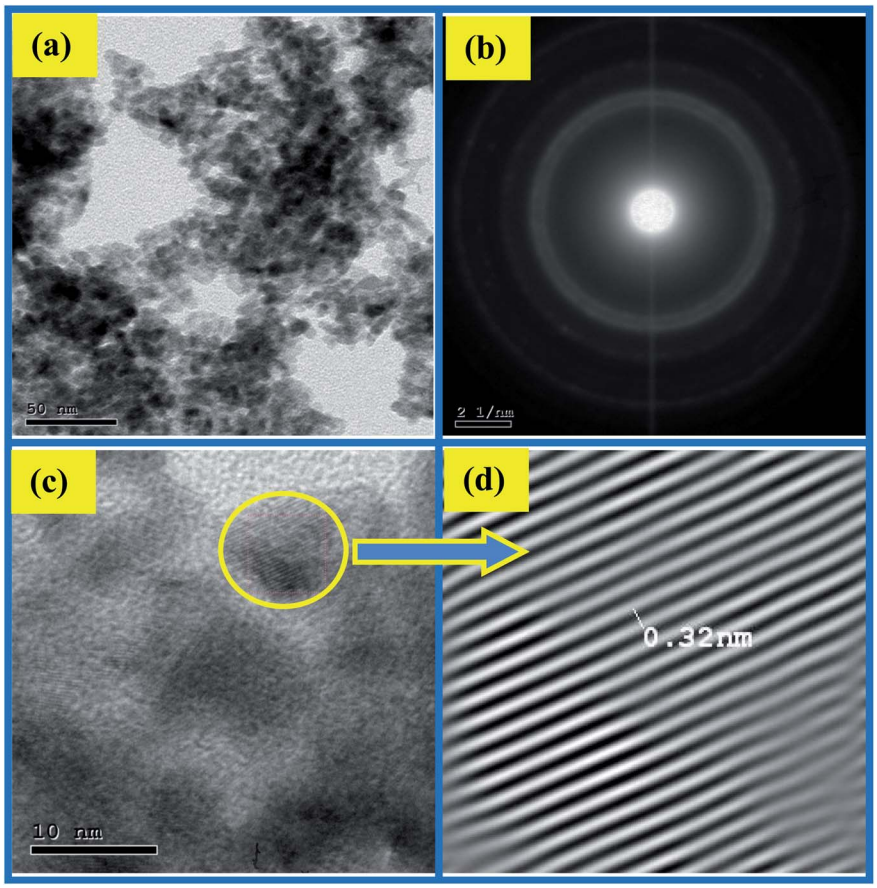

Fig. 5 (a) TEM, (b) SAED and (c and d) HR-TEM of CuO sample prepared in pure ethanol.

spacing between the (11−1) planes of the monoclinic CuO structure.

3.4. Structural analysis

Structural analysis of three CuO samples prepared using different ethanol content in water *i.e.* 0%, 50%, and 100% was done *via* Rietveld method, the profile fits are illustrated in Fig. 6. It is clear that both of the observed and calculated patterns are fit well as indicated by R values (Table 1). Noticeably, all the reflections are matched well and there are no other reflections that can be related to the existence of Cu_2O. The refinement results shown in Table 1 reveals a pronounced influence of the ethanol content on the monoclinic unit cell parameters. Elongation in "a" and "c" occurs with increasing of ethanol content, largest values are adopted by the sample formed in pure ethanol. Moreover, this sample shows also the largest volume of the monoclinic unit cell. These variations in the cell parameters are of course a result of the difference in both of the particle size and morphological shape of the so obtained CuO NPs.

On the other hand, the internal local strain (ε)[31] and dislocation density (δ)[32] of the three CuO samples were estimated by the following relations:

$$\varepsilon = \frac{\beta \cos \theta}{4} \quad (3)$$

$$\delta = \frac{1}{D^2} \text{lines per m}^2 \quad (4)$$

where, β is the full width at half-maximum intensity (FWHM), θ is the Bragg diffraction angle in degrees and D is the average crystallite size.

Table 2 shows the variation of ε and δ with ethanol content in water. There is an increase in both of the internal local strain (ε) and the dislocation density (δ) with increasing of ethanol content which is related mainly to the decrease in the average particle size.

3.5. BET surface area

The surface texture of CuO NPs (prepared using different ethanol content *i.e.* 0%, 50%, and 100%) was examined *via* the nitrogen adsorption–desorption process. The BET method was applied and the isotherms are shown in Fig. 7. The obtained isotherms can be classified as type IV,[33] with a hysteresis characterizes this type and which implies the presence of mesopores. In this type, the capillary condensation associated with the mesopores limits the adsorption at a high P/P°. The hysteresis seen in the isotherms depicted in Fig. 7a and b can be classified as H3 type that does not display any limiting adsorption at high P/P°. Furthermore, the hysteresis shown in Fig. 7c is classified as H2 type, which suggests pores with

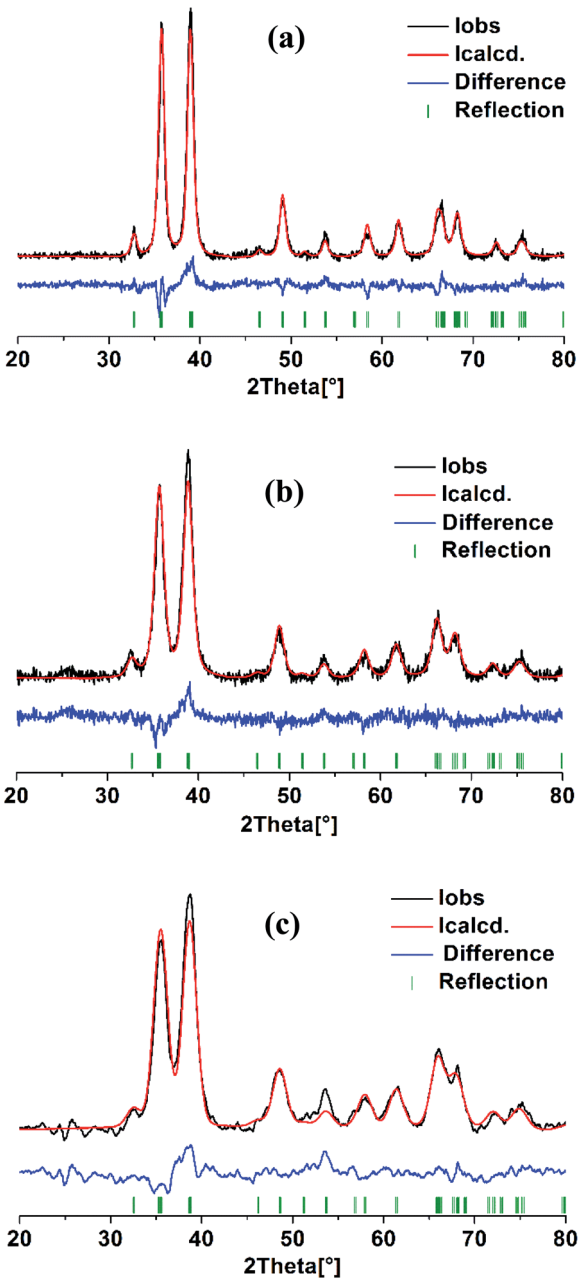

Fig. 6 Rietveld refinement analysis of CuO samples prepared in solutions with different ethanol content: (a) 0%, (b) 50% and (c) 100%.

narrow necks and wide bodies. The lowest BET surface area was adopted by the CuO sample prepared in pure water (90.5 m^2 g^{-1}) and that has a rod-like morphology. Increase of the surface area occurs with increasing of ethanol content in water. Nonetheless, the sample prepared in pure ethanol with a sphere-like shape exhibits a surface area (103 m^2 g^{-1}) lower than that obtained in 50% ethanolic solution (146 m^2 g^{-1}). The average pore width for the three samples was determined, the lowest one was for the sample prepared in ethanol. The average pore widths of the samples are 7.8, 5.9, and 4.8 nm, which indicate the presence of mesoporous texture. Pore volume was determined also, the largest one was adopted by the sample obtained in 50% EtOH/H_2O. This could be the reason why it has an unanticipated larger surface area than the sample obtained in pure ethanol. For the later, the smaller measured surface area than expected may be also due to the presence of acetate ions bound to its surface although, it was preheated to 150 °C prior to surface area measurements. Table 3 presents the detailed physicochemical properties of CuO NPs prepared using different ethanol content.

Table 1 Measurement parameters, structure and refinement data of three CuO samples obtained using different ethanol content in water

	0%	50%	100%
a/Å	4.683(1)	4.697(2)	4.711(3)
b/Å	3.422(1)	3.414(2)	3.417(2)
c/Å	5.134(1)	5.134(3)	5.155(3)
β°	99.25(1)	99.29(3)	99.36(3)
V/(Å)^3	81.207	81.25	81.869
R (expected)/%	4.267	4.856	5.947
R (profile)/%	6.328	6.958	6.861
R (weighted profile)/%	8.018	8.665	8.669
R (Bragg)/%	4.975	4.370	5.207
GOF	3.532	3.184	2.125

3.6. Thermal behavior

Thermogravimetric studies were carried out by subjecting CuO NPs (prepared in pure water, pure ethanol, and 50% EtOH/H_2O) to non-isothermal heat-treatment from 25–800 °C with a heating rate of 5 °C min^{-1}. The corresponding TGA curves are depicted in Fig. 8a whereas their DTA curves are shown in Fig. 8b. For the sample obtained in pure water, a small weight loss of 0.80% is observed in the first step (25–120 °C), which could be due to the evaporation of adsorbed moisture on the surface of the nanoparticles. The second tiny mass loss (~1%) seen at 120–400 °C could be related to the elimination of unreacted acetate ions (from the start materials). The presence of adsorbed acetates on the surface of nanoparticles was proven formerly by IR analysis. DTA analysis showed an endothermic peak at ~80 °C which corresponds to the 1st step whereas, an exothermic peak is observed at 229 °C that is associated with the 2nd step. On the other hand, TGA analysis of the sample formed in pure ethanol displayed a different behavior. Large mass loss of ~2% is obvious in 1st step which is related to the removal of the adsorbed water and/or ethanol. In the second step, the mass loss of 4.5% observed in a temperature range of 150–500 °C with an exothermic peak at

Table 2 Variation of the average particle size (estimated from XRD lines and TEM measurements), lattice strain and dislocation density with the variation of ethanol content in water

	0%	50%	100%
D_{TEM}/nm	15.0	—	7.0
D_{XRD}/nm	13.0	9.4	7.2
$\varepsilon \times 10^{-3}$	2.78	3.83	4.64
$\delta \times 10^{16}$ line per m^2	0.592	1.13	1.93

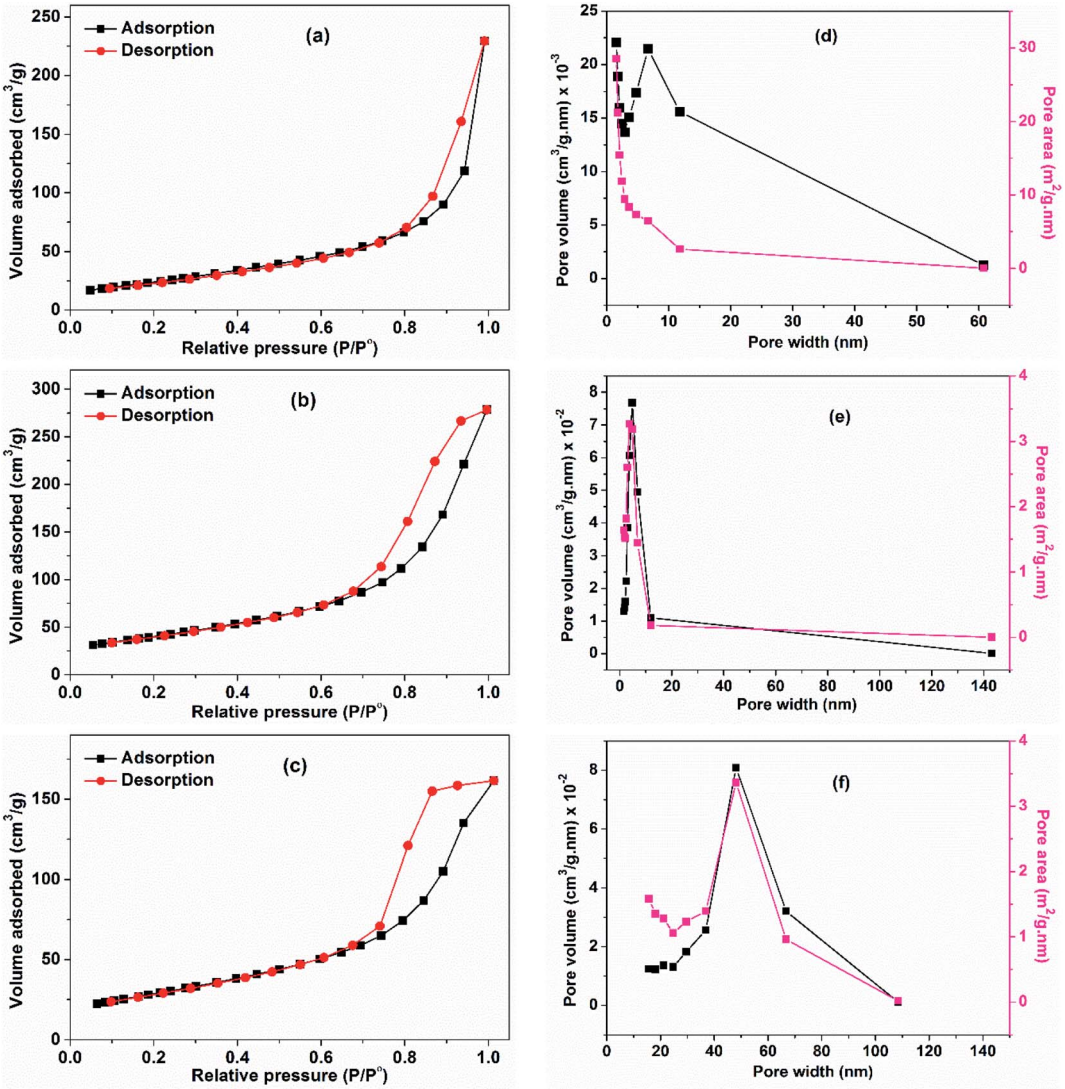

Fig. 7 Adsorption–desorption isotherms of CuO samples prepared using different ethanol content: (a) 0%, (b) 50% and (c) 100%. (d–f) Their pore-volume and pore-area distribution curves, respectively.

222 °C reveals a higher extent of the adsorbed acetate on the surface of this sample. These results are coinciding with the IR results. For the sample obtained in 50% ethanolic solution (with moderate content of acetates and ethanol adsorbed on its surface) a similar behavior was observed, however, with smaller mass losses than those observed for the sample obtained in pure ethanol.

3.7. Optical absorption and energy gap of CuO NPs

The optical properties of X-ray single-phase CuO nanostructures were studied by recording the UV-vis absorption spectra of the prepared CuO samples dispersed in water. The suspensions showed reasonable stability during the measurements and no visible sedimentation was observed. The sample obtained in ethanol exhibited the highest colloidal stability that could be attributed to the presence of a large extent of the negatively charged acetate ions adsorbed on the NPs surface as shown

Table 3 Surface area, average pore width and total pore volume for CuO sample prepared in different % EtOH/H_2O

EtOH/H_2O	S_{BET} ($m^2\ g^{-1}$)	External surface area ($m^2\ g^{-1}$)	Average pore width (nm)	Total pore volume ($cm^3\ g^{-1}$)
0%	90.5	90.5	7.8	0.35
50%	145.0	145.5	5.9	0.43
100%	103.0	103.0	4.8	0.25

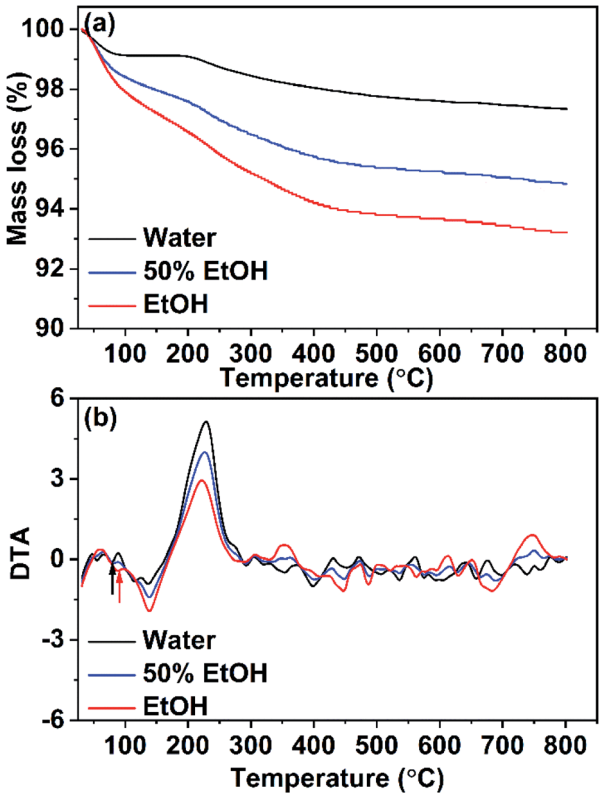

Fig. 8 (a) TGA and (b) DTA analyses for CuO samples prepared in pure water and pure ethanol and in a mixture of them.

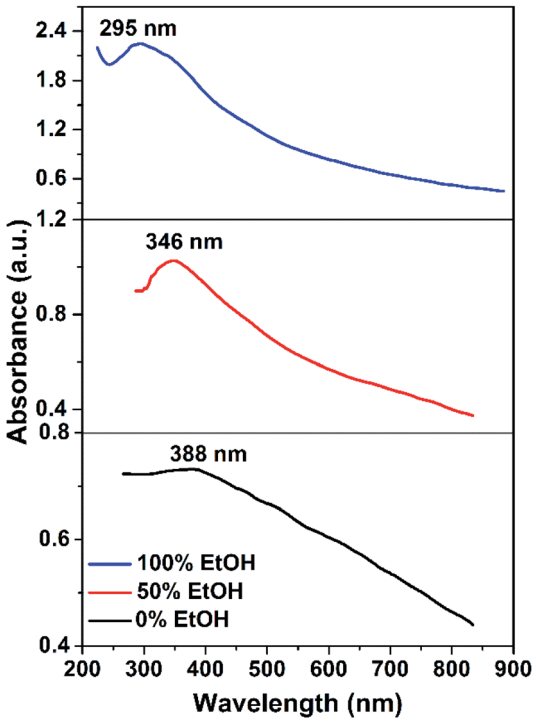

Fig. 9 UV-vis spectra of CuO samples prepared in solutions with different ethanol content.

before by IR and TGA results. This of course leads to electrostatic repulsions among the particles and hence rises the colloidal stability. The absorption spectra of the samples, synthesized in pure water, ethanol and in a mixture of them (50% v/v) showed broad absorption peaks revealing their high absorption character. For the sample obtained in pure water (Fig. 9), absorption peak is apparent at $\lambda_{max} = 388$ nm that is related to the electronic transition from the valence to the conduction band. This band is a characteristic band for CuO, however, some reports showed the appearance of an additional broad band at ~620 nm.[34–36] In our case, we are not able to see this band could be due to the size and shape effect. Actually, the optical properties of CuO are function of several parameters such as size, shape, sample preparation, and measurement technique.[37] A blue shift in the peak position (*i.e.* 388, 346, and 295 nm) is seen while the water is partially replaced by ethanol. The optical gap energy values were determined by using Tauc's relationship:[38]

$$\alpha h\nu = C(h\nu - E_g)^n \quad (5)$$

where C is a characteristic constant related to the material, $h\nu$ is the photon energy in eV, α is the absorption coefficient in cm^{-1} and the exponent n equals $\frac{1}{2}$ or 2 for direct or indirect optical transition, respectively.

Tauc's plots of $(\alpha h\nu)^2$ *versus* photon energy $h\nu$ are illustrated in Fig. 10 which reveals the predominant direct transition of the prepared CuO nanostructures. The intercept of the $(\alpha h\nu)^2$ with $h\nu$ axis at $(\alpha h\nu)^2 =$ zero gives the values of E_g. Obviously, E_g value increases from 2.2 to 2.65 eV while the reaction solvent has changed from pure water to pure ethanol. Meanwhile, E_g of 2.35 eV is found for the sample obtained in 50% (v/v) ethanol/water solution. This blue shift in the value of the energy gap could be related to the quantum confinement phenomena associated with the particle size reduction as a function of ethanol content in water. Actually, the photocatalytic activity of any photocatalyst is much affected by the band gap value. The larger band gap value, the slower the electron–hole recombination rate. Accordingly, electrons and holes generated (charge carriers) in the bulk will be allowed to reach the photocatalyst

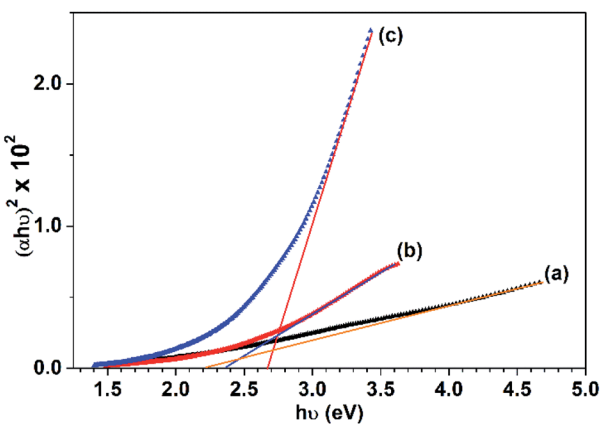

Fig. 10 Tauc's plots for the CuO samples prepared in: (a) 0%, (b) 50% and (c) 100% (v/v) ethanol/water solutions.

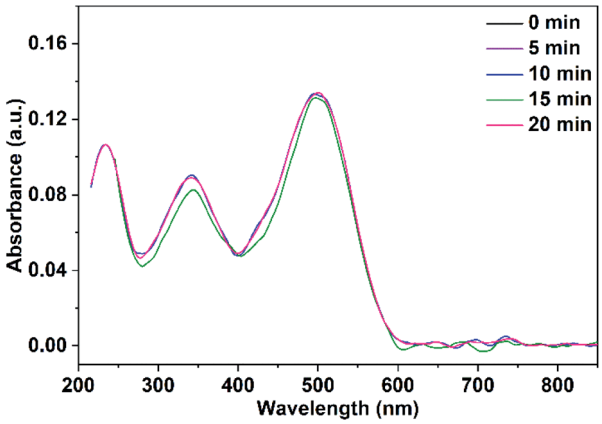

Fig. 11 UV-vis spectra of Congo red illuminate with UV-LED lamp over 20 min in the absence of the photocatalyst.

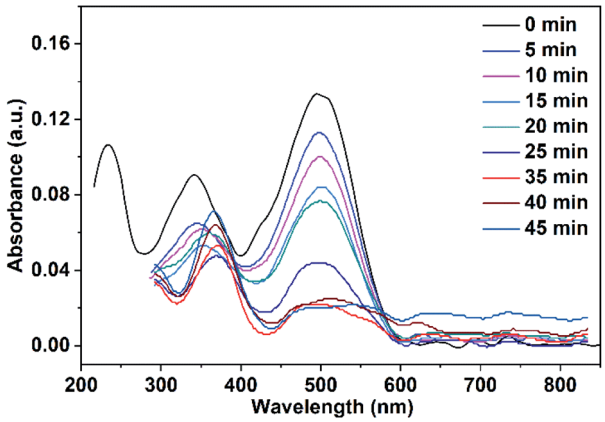

Fig. 12 UV-vis spectra of Congo red (75 mL, 5 ppm) illuminate with UV-LED lamp in the presence of 10 mg CuO NPs prepared in pure ethanol.

surface and participate in the photoreactions. Therefore, it is expected here that CuO NPs obtained in ethanol will have better photocatalytic activity than those obtained in water. However, among the other factors that influence the rate of recombination between the holes and the electrons are: crystal size, surface area, defect population, and porosity. Hence, any difference in these features between both CuO NPs can result in a substantial change in their photocatalytic activity.

3.8. Photocatalytic removal of Congo red

The adsorbed quantity of organic pollutants on the surface of nanoparticles has a significant impact on their photocatalytic efficiency. Consequently, the adsorption of Congo red on CuO NPs in the dark was tracked by taking absorbance measurements at various time intervals. In the absence of UV irradiation and after a contact time of 30 min between Congo red and CuO NPs, the determined rate constants were 0.0017, and 0.002 min^{-1} for CuO NPs obtained in pure water and ethanol, respectively.

Before the study of the photocatalytic activity of the prepared CuO NPs, a blank solution of the Congo red dye was illuminated with a UV-LED lamp of a power 11.8 W (λ = 365 nm) in the absence of the photocatalyst. As observed in Fig. 11, three absorption maxima are present in the UV-vis spectrum of Congo red. The irradiation of the dye over 20 min does not result in a variation of its concentration. In the next step, a mixture of the dye solution (75 mL of 5 ppm dye concentration) and 10 mg of CuO NPs (prepared in pure ethanol and pure water) was kept in dark for 30 min to establish the adsorption–desorption equilibrium. The mixture was then irradiated with the UV-LED lamp over 45 min. Portions of 5 mL of the mixture were taken over different time intervals after elimination of the solid nanoparticles. The remained concentration of the dye in the different portions was determined (using the calibration curve built up for different dye concentrations and shown in Fig. S1†) by recording their UV-vis spectra. The received spectra shown in Fig. 12 and 13 reveal the effect of irradiation time on the dye concentration, drop of the dye concentration (*i.e.* decrease of the dye absorbance) occurs with increasing of irradiation time. This finding demonstrates the effect of the photocatalyst on the dye removal, the dye color gets fainter and fainter with increasing of irradiation time.

It is clear from Fig. 12 and 13 that the absorption peak at λ_{max} = 499 nm vanishes with time. On the other hand, the peak at λ_{max} = 342 nm has been disappeared and instead a new peak at λ_{max} = 372 nm has appeared. This result reflects the degradation of the Congo red molecule and the formation of small non-toxic organic molecules. Removal efficiency (R%) of Congo red was calculated *via* the following equation:

$$R(\%) = \frac{C_i - C_e}{C_i} \times 100 \quad (6)$$

where C_i and C_e (mg L^{-1}) are the initial and the equilibrium concentrations of the Congo red solution, respectively.

The efficiency of CuO NPs prepared in pure ethanol and pure water for removal of the dye increases with the time of irradiation as shown in Fig. 14. Obviously, during the first 25 min, the CuO NPs prepared in pure water show more efficient removal for the dye color compared to that of the prepared NPs in pure

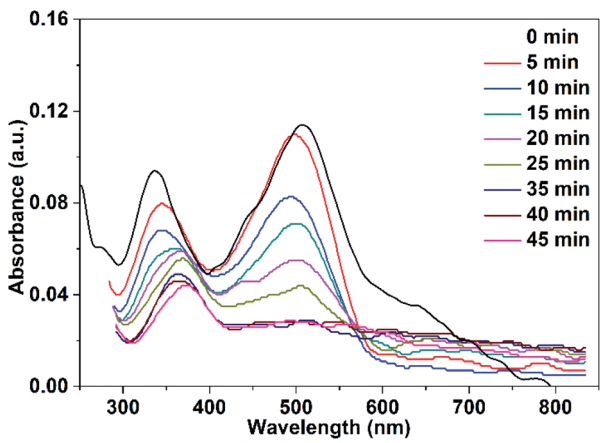

Fig. 13 UV-vis spectra of Congo red (75 mL, 5 ppm) illuminate with UV-LED lamp in the presence of 10 mg CuO NPs prepared in pure water.

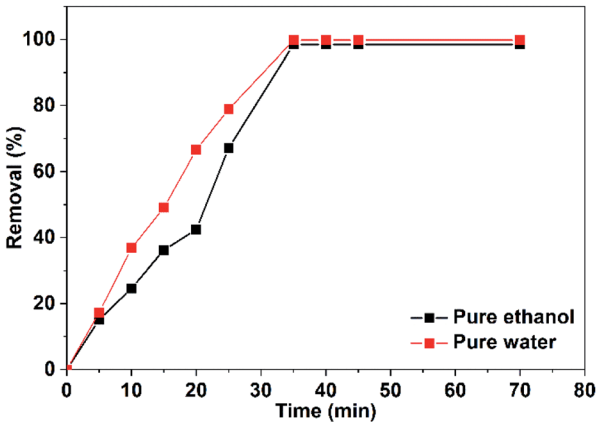

Fig. 14 Efficacy of the photocatalytic removal of Congo red (75 mL, 5 ppm) in the presence of 10 mg of CuO NPs prepared in pure ethanol and pure water.

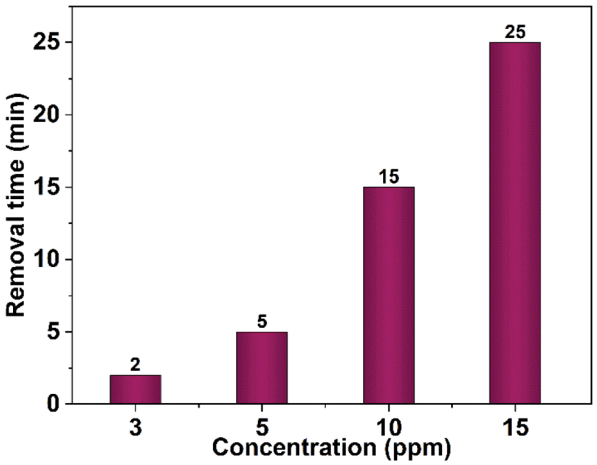

Fig. 16 Effect of the dye concentration on the time needed for complete removal of Congo red (75 mL), 40 mg CuO NPs obtained in pure ethanol was employed.

ethanol. This could be related to the presence of the acetate ions bounded to the surface of the nanoparticles obtained in pure ethanol that repel and hinder the accumulation of the anionic dye molecules over the NPs surface. For both CuO samples, approximately complete decolorization of the dye occurs in 35 min as depicted in Fig. 14.

The impact of the dose of the photocatalyst on the dye remediation was studied employing different weights of CuO NPs prepared in pure ethanol. The results showed that increasing of the catalyst weight results in a drop of the time required for complete dye removal. As shown in Fig. 15 a complete dye removal is accomplished in 35 min using 10 mg of the photocatalyst. However, by rising the dose to 60 mg the time necessary for elimination of the whole dye color reaches 2 min.

Furthermore, the effect of the dye concentration on the time required for complete dye removal was also examined. The results revealed an increase in the time necessary for the entire dye removal with rising of the dye concentration as shown in Fig. 16. Studying the impact of the pH of the medium showed that degradation considerably decreases in the alkaline pH region as shown in Fig. 17. Acidic or neutral pHs are optimum media for the entire dye removal.

3.8.1. Kinetic studies. The kinetics of photocatalytic degradation of Congo red was examined by the Langmuir–Hinshelwood (L–H) model. L–H model correlates the rate of degradation (r) of an organic compound in water and its concentration (c) at time t as given below:[39–41]

$$r = -\frac{dc}{dt} = \frac{k_r K_{ad}}{1 + K_{ad} C} \quad (7)$$

where k_r and K_{ad} are the rate and the adsorption equilibrium constants, respectively. Omitting the denominator and taking into consideration that C_0 (the concentration at $t = 0$) is very small, the reaction is principally a pseudo-first order reaction. Therefore, the following relation is received:

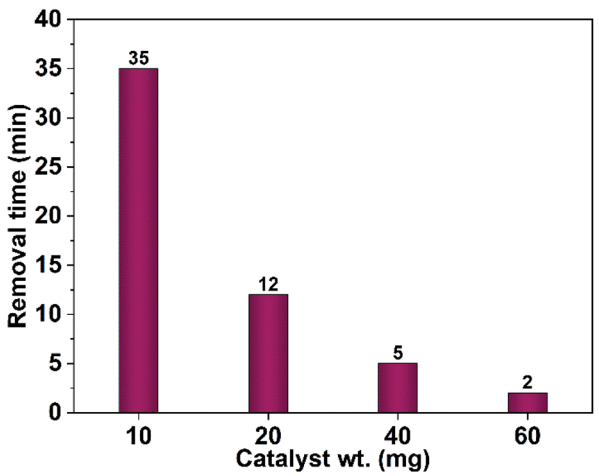

Fig. 15 Effect of the photocatalyst dose (CuO NPs obtained in pure ethanol) on the time needed for complete removal of Congo red (75 mL, 5 ppm).

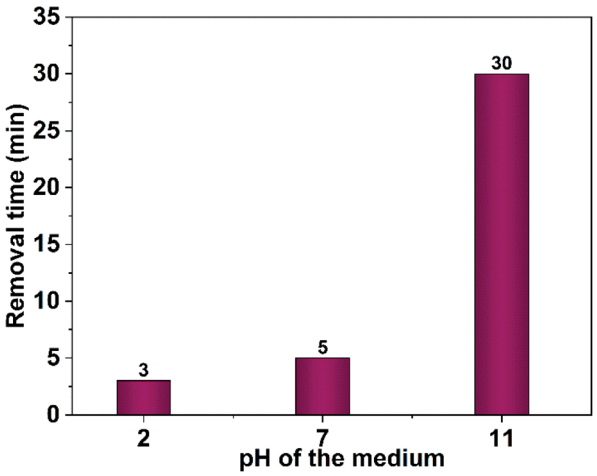

Fig. 17 Effect of medium pH on photodegradation time of Congo red (75 mL, 5 ppm), 40 mg CuO NPs obtained in pure ethanol was employed.

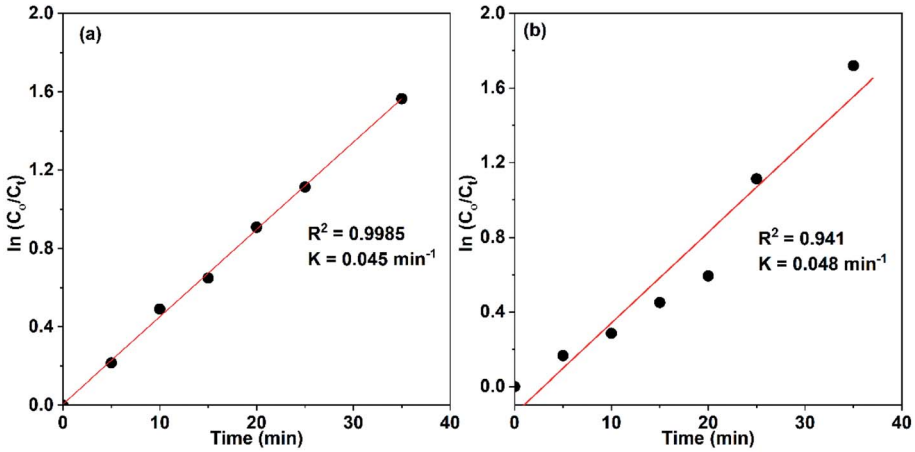

Fig. 18 Kinetics of photocatalytic degradation of Congo red (75 mL, 5 ppm) using 10 mg CuO NPs as photocatalysts that are prepared in: (a) water and (b) ethanol.

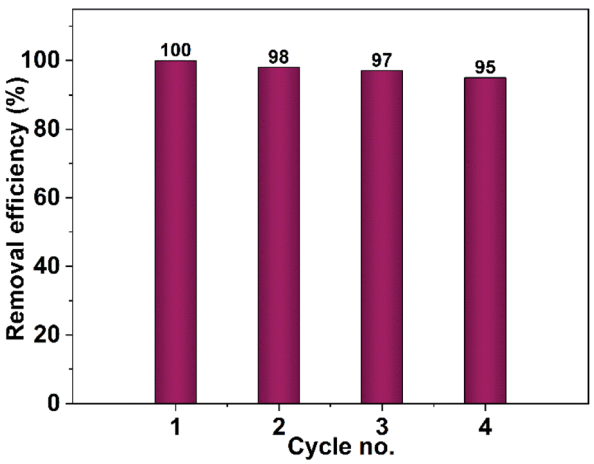

Fig. 19 Recyclability test of CuO photocatalyst obtained from pure ethanol for the removal of Congo red.

$$\ln\left(\frac{C_0}{C}\right) = k_r K_{ad} t = k_{app} t \quad (8)$$

where k_{app} is the apparent first-order rate constant.

Accordingly, the apparent rate constant is found from the slope of the plot of $\ln(C_0/C)$ *versus* t. The results showed that the degradation of Congo red using CuO NPs obtained in water follows typically the pseudo-first-order kinetics as established by the obtained linearity of the plot shown in Fig. 18a, rate constant of 0.045 min^{-1} was found. On the other hand, for the sample obtained in ethanol, the plot shown in Fig. 18b reveals a little bite deviation of the obtained data nonetheless we still could fit them linearly. A first-order rate constant of 0.048 min^{-1} was found for this sample.

3.8.2. Photodegradation mechanism. The electron and hole pairs (e_{CB}^-/h_{VB}^+) are produced while exposing CuO to UV light. The photocatalysis process takes place essentially on the surface of CuO, where the photo-produced electrons and holes are trapped.[42] During the course of the reaction, the superoxide radical ($O_2^{\bullet -}$) is generated as a result of the reaction between electron and adsorbed oxygen. The superoxide radical can perform as an oxidant or reductant. However, the reaction between holes and adsorbed H_2O or hydroxide groups in the aqueous media leads to the production of hydroxyl radical ($^{\bullet}OH$), which is a powerful oxidant.[43] The reactive species generated during CuO photocatalysis *i.e.*, h_{VB}^+, e_{CB}^-, $^{\bullet}OH$, $O_2^{\bullet -}$, $^{\bullet}O_2H$, H_2O_2, $^1O_2$, *etc.* can result in the destruction of the pollutants under investigation.

The photocatalytic elimination of Congo red was performed in the existence of either isopropanol or Na_2EDTA as $^{\bullet}OH$ and

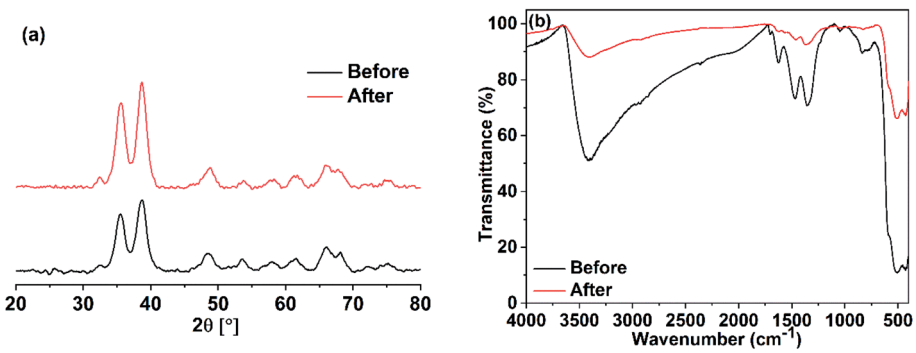

Fig. 20 (a) XRD and (b) IR analyses of CuO nano-photocatalyst obtained in ethanol before and after catalytic cycles.

hole scavengers, respectively. The results revealed a drop in the efficiency of removal to ~85 and 80%, respectively. This result may indicate that both $^{\bullet}OH$ radicals and holes have a moderate reactivity in the photocatalytic removal of Congo red. Moreover, superoxide radicals could be the species with the major responsibility for performing the photo-degradation of the Congo red molecules.

3.8.3. Recycling and stability of the photocatalyst. The reusability of CuO photocatalyst obtained from pure ethanol was examined. Separation of the photocatalyst was made next to the first cycle, washed with water and ethanol, and dried overnight. The photocatalyst was employed once again in the successive photocatalytic cycles. The results perceived in Fig. 19 reveal that after further three cycles the photocatalytic efficiency of CuO NPs is slightly reduced.

The stability of the prepared photocatalyst (CuO obtained in ethanol) was examined by XRD and IR analyses after it has been carefully washed. The XRD and IR results demonstrated in Fig. 20 showed that our photocatalyst is stable and no change in its structure could be seen.

4. Conclusion

Successfully CuO NPs were obtained *via* simple sol–gel method in ethanol–water mixed solvents. Variation of the ethanol content in water results in nanoparticles with different sizes and shapes. The particle size drops drastically from 13 to 7 nm while the water is completely replaced by ethanol. Moreover, the particles had a rod-like shape in pure water and a spherical shape in pure ethanol. The obtained results revealed that the variation of CuO particle size and morphology had an enormous effect on their physico-chemical properties. Structural studies showed the enlargement of the monoclinic unit cell volume with the replacement of water by ethanol. Furthermore, the internal local strain (ε) and the dislocation density (δ) were increased with increasing of ethanol content. The largest optical band gap was adopted by the CuO NPs prepared in pure ethanol. The photocatalytic study showed that CuO NPs prepared in pure water had a higher efficacy for Congo red removal (during the first 25 min) than those obtained in pure ethanol. For both, the removal of the entire dye color was accomplished in 35 min.

Finally, the presence of ethanol and adsorbed acetate as templating agents leads to the variation of both the particle size and morphology of the obtained CuO NPs. Furthermore, the water/ethanol percentage plays a crucial role in the tuning of structural, optical and photocatalytic properties of the synthesized CuO nanoparticles for the potential applications in wastewater treatment.

Conflicts of interest

The authors declare no conflict of interest

References

1 M. Fernández-García, A. Martínez-Arias, J. C. Hanson and J. A. Rodriguez, Nanostructured oxides in chemistry: characterization and properties, *Chem. Rev.*, 2004, **104**, 4063–4104.

2 K. J. Choi and H. W. Jang, One-dimensional oxide nanostructures as gas-sensing materials: review and issues, *Sensors*, 2010, **10**, 4083–4099.

3 M. M. Rahman, A. J. S. Ahammad, J.-H. Jin, S. J. Ahn and J.-J. Lee, A Comprehensive review of glucose biosensors based on nanostructured metal-oxides, *Sensors*, 2010, **10**, 4855–4886.

4 S. B. Wang, C. H. Hsiao, S. J. Chang, K. T. Lam, K. H. Wen, S. C. Hung, S. J. Young and B. R. Huang, A CuO nanowire infrared photodetector, *Sens. Actuators, A*, 2011, **171**, 207–211.

5 R. V. Kumar, Y. Diamant and A. Gedanken, Sonochemical synthesis and characterization of nanometer-size transition metal oxides from metal acetates, *Chem. Mater.*, 2000, **12**, 2301–2305.

6 X. Zhang, W. Shi, J. Zhu, D. J. Kharistal, W. Zhao, B. S. Lalia, H. H. Hng and Q. Yan, High-power and high-energy-density flexible pseudocapacitor electrodes made from porous CuO nanobelts and single-walled carbon nanotubes, *ACS Nano*, 2011, **5**, 2013–2019.

7 J. Liu, J. Jin, Z. Deng, S.-Z. Huang, Z.-Y. Hu, L. Wang, C. Wang, L.-H. Chen, Y. Li, G. Van Tendeloo and B.-L. Su, Tailoring CuO nanostructures for enhanced photocatalytic property, *J. Colloid Interface Sci.*, 2012, **384**, 1–9.

8 I. Ali, New generation adsorbents for water treatment, *Chem. Rev.*, 2012, **112**, 5073–5091.

9 X.-Y. Yu, R.-X. Xu, C. Gao, T. Luo, Y. Jia, J.-H. Liu and X.-J. Huang, Novel 3D hierarchical cotton-candy-Like CuO: surfactant-free solvothermal synthesis and application in As(III) removal, *ACS Appl. Mater. Interfaces*, 2012, **4**, 1954–1962.

10 A. Azam, A. S. Ahmed, M. Oves, M. S. Khan and A. Memic, Size-dependent antimicrobial properties of CuO nanoparticles against Gram-positive and -negative bacterial strains, *Int. J. Nanomedicine*, 2012, **7**, 3527–3535.

11 P. Mallick and S. Sahu, Structure, microstructure and optical absorption analysis of CuO nanoparticles synthesized by sol-gel route, *Nanosci. Nanotechnol.*, 2012, **2**, 71–74.

12 T. Jiang, Y. Wang, D. Meng, X. Wu, J. Wang and J. Chen, Controllable fabrication of CuO nanostructure by hydrothermal method and its properties, *Appl. Surf. Sci.*, 2014, **311**, 602–608.

13 P. Pookmanee, P. Sangthep, J. Tafun, V. Kruefu, S. Kojinok and S. Phanichphant, Synthesis of copper oxide nanopowder by microwave method, *Solid State Phenom.*, 2018, **283**, 154–159.

14 M. I. Said, A. I. El-Said, A. A. M. Aly and A. Abou-Taleb, Ultrasound assisted facile synthesis of Mn(II) and Cu(II) coordination polymers and their use as precursors for α-

Mn_3O_4 and CuO nanoparticles: synthesis, characterization and catalytic properties, *Ultrason. Sonochem.*, 2018, **46**, 68–78.
15 J. Zhu, H. Bi, Y. Wang, X. Wang, X. Yang and L. Lu, CuO nanocrystals with controllable shapes grown from solution without any surfactants, *Mater. Chem. Phys.*, 2008, **109**, 34–38.
16 G. Oskam, Metal oxide nanoparticles: synthesis, characterization and application, *J. Sol-Gel Sci. Technol.*, 2006, **37**, 161–164.
17 A. Iribarren, E. Hernández-Rodríguez and L. Maqueira, Structural, chemical and optical evaluation of Cu-doped ZnO nanoparticles synthesized by an aqueous solution method, *Mater. Res. Bull.*, 2014, **60**, 376–381.
18 M. Zhang, Y. Bando and K. Wada, Sol-gel template preparation of TiO_2 nanotubes and nanorods, *J. Mater. Sci. Lett.*, 2001, **20**, 167–170.
19 K. Woo, H. J. Lee, J.-P. Ahn and Y. S. Park, Sol–gel mediated synthesis of Fe_2O_3 nanorods, *Adv. Mater.*, 2003, **15**, 1761–1764.
20 M. Kashif, S. M. Usman Ali, M. E. Ali, H. I. Abdulgafour, U. Hashim, M. Willander and Z. Hassan, Morphological, optical, and Raman characteristics of ZnO nanoflakes prepared via a sol–gel method, *Phys. Status Solidi A*, 2012, **209**, 143–147.
21 J. Li, Y. Wu, M. Yang, Y. Yuan, W. Yin, Q. Peng, Y. Li and X. He, Electrospun Fe_2O_3 nanotubes and Fe_3O_4 nanofibers by citric acid sol-gel method, *J. Am. Ceram. Soc.*, 2017, **100**, 5460–5470.
22 S. Maensiri, W. Nuansing, J. Klinkaewnarong, P. Laokul and J. Khemprasit, Nanofibers of barium strontium titanate (BST) by sol–gel processing and electrospinning, *J. Colloid Interface Sci.*, 2006, **297**, 578–583.
23 M. I. Said and B. Harbrecht, Size-controlled synthesis of Mn_3O_4 nanoparticles: characterization and defect chemistry, *J. Nanopart. Res.*, 2019, **21**, 1–15.
24 S. J. Iyengar, M. Joy, A. P. Mohamed, S. Samanta, C. K. Ghosh and S. Ghosh, Fabrication of magnetite nanocrystals in alcohol/water mixed solvents: catalytic and colloid property evaluation, *RSC Adv.*, 2016, **6**, 60845–60855.
25 K. Davis, R. Yarbrough, M. Froeschle, J. White and H. Rathnayake, Band gap engineered zinc oxide nanostructures via a sol–gel synthesis of solvent driven shape-controlled crystal growth, *RSC Adv.*, 2019, **9**, 14638–14648.
26 P. Janos, H. Buchtova and M. Ryznarova, Sorption of dyes from aqueous solutions onto fly ash, *Water Res.*, 2003, **37**, 4938–4944.
27 S. Seshadri, P. L. Bishop and A. M. Agha, Anaerobic/aerobic treatment of selected azo dyes in wastewater, *Waste Manage.*, 1994, **14**, 127–137.
28 S. Rehman, A. Mumtaz and S. K. Hasanain, Size effects on the magnetic and optical properties of CuO nanoparticles, *J. Nanopart. Res.*, 2011, **13**, 2497–2507.
29 R. A. Nyquist and R. O. Kagel, *Infrared Spectra of Inorganic Compounds*, Academic Press, 1997, p. 220.
30 G. Kliche and Z. V. Popovic, Far-infrared spectroscopic investigations on CuO, *Phys. Rev. B: Condens. Matter Mater. Phys.*, 1990, **42**, 10060–10066.
31 P. P. Hankare, P. A. Chate, D. J. Sathe, P. A. Chavan and V. M. Bhuse, Effect of thermal annealing on properties of zinc selenide thin films deposited by chemical bath deposition, *J. Mater. Sci.: Mater. Electron.*, 2009, **20**, 374–379.
32 B. D. Cullity, *Elements of X-ray Diffraction, Chemical Analysis by Diffraction*, 1956.
33 D. H. Everett, Manual of Symbols and Terminology for Physicochemical Quantities and Units, Appendix II: Definitions, Terminology and Symbols in Colloid and Surface Chemistry, *Pure Appl. Chem.*, 1972, 577.
34 J. Jayaprakash, N. Srinivasan, P. Chandrasekaran and E. K. Girija, Synthesis and characterization of cluster of grapes like pure and zinc-doped CuO nanoparticles by sol–gel method, *Spectrochim. Acta, Part A*, 2015, **136**, 1803–1806.
35 P. Kumar, M. C. Mathpal, J. Prakash, B. C. Viljoen, W. D. Roos and H. C. Swart, Band gap tailoring of cauliflower-shaped CuO nanostructures by Zn doping for antibacterial applications, *J. Alloys Compd.*, 2020, **832**, 154968.
36 P. Kumar, G. K. Inwati, M. C. Mathpal, S. Ghosh, W. D. Roos and H. C. Swart, Defects induced enhancement of antifungal activities of Zn doped CuO nanostructures, *Appl. Surf. Sci.*, 2021, **560**, 150026.
37 Q. Zhang, K. Zhang, D. Xu, G. Yang, H. Huang, F. Nie, C. Liu and S. Yang, CuO nanostructures: synthesis, characterization, growth mechanisms, fundamental properties, and applications, *Prog. Mater. Sci.*, 2014, **60**, 208–337.
38 J. Tauc, *Amorphous and Liquid Semiconductors*, Springer US, Boston, MA, 1974.
39 A. V. Petukhov, Effect of molecular mobility on kinetics of an electrochemical Langmuir-Hinshelwood reaction, *Chem. Phys. Lett.*, 1997, **277**, 539–544.
40 B. Bayarri, J. Giménez, D. Curcó and S. Esplugas, Photocatalytic degradation of 2,4-dichlorophenol by TiO_2/UV: kinetics, actinometries and models, *Catal. Today*, 2005, **101**, 227–236.
41 E. Kusvuran, A. Samil, O. M. Atanur and O. Erbatur, Photocatalytic degradation kinetics of di- and tri-substituted phenolic compounds in aqueous solution by TiO_2/UV, *Appl. Catal., B*, 2005, **58**, 211–216.
42 J. Tang, J. R. Durrant and D. R. Klug, Mechanism of photocatalytic water splitting in TiO_2. Reaction of water with photoholes, importance of charge carrier dynamics, and evidence for four-hole chemistry, *J. Am. Chem. Soc.*, 2008, **130**, 13885–13891.
43 U. I. Gaya and A. H. Abdullah, Heterogeneous photocatalytic degradation of organic contaminants over titanium dioxide: a review of fundamentals, progress and problems, *J. Photochem. Photobiol., C*, 2008, **9**, 1–12.